In: Algorithms for Synthetic Aperture Radar Imagery XV (Proceedings of SPIE vol. 6970), SPIE Defense and Security Symposium, March 2008.

Recursive SAR Imaging

Randolph L. Moses and Joshua N. Ash
Ohio State University, Dept. of Electrical and Computer Engineering, Columbus, OH, USA

ABSTRACT

We investigate a recursive procedure for synthetic aperture imaging. We consider a concept in which a SAR system persistently interrogates a scene, for example as it flies along or around that scene. In traditional SAR imaging, the radar measurements are processed in blocks, by partitioning the data into a set of non-overlapping or overlapping azimuth angles, then processing each block. We consider a recursive update approach, in which the SAR image is continually updated, as a linear combination of a small number of previous images and a term containing the current radar measurement. We investigate the crossrange sidelobes realized by such an imaging approach. We show that a first-order autoregression of the image gives crossrange sidelobes similar to a rectangular azimuth window, while a third-order autoregression gives sidelobes comparable to those obtained from widely-used windows in block-processing image formation. The computational and memory requirements of the recursive imaging approach are modest—on the order of $M \cdot N^2$ where M is the recursion order (typically ≤ 3) and N^2 is the image size. We compare images obtained from the recursive and block processing techniques, both for a synthetic scene and for X-band SAR measurements from the Gotcha data set.

Keywords: synthetic aperture radar, SAR, recursive, SAR imaging, SAR video, convolution backprojection imaging

1. INTRODUCTION

Synthetic aperture radar (SAR) is widely used for surveillance and has application in many areas, including land mapping, environmental monitoring, remote mapping, and surveillance. Traditional SAR imaging entails a mobile radar system (mounted on an aircraft or satellite, for example) that interrogates a scene of interest. Radar images are formed by processing the data over a contiguous set of collection samples. Algorithms such as convolution backprojection (CBP) or the Polar Format Algorithm (PFA) are typically used.[1,2]

Recently there has been an increased interest in SAR systems that persistently sense a scene of interest. One concept is that of an airborne platform that flies continuous circles around the center of a scene of interest, and forms a continual set of SAR images of that scene. These images may be registered and viewed as a movie, a process sometimes called "SAR video."

This paper considers recursive processing techniques that can be used for SAR video applications. The basic idea is to consider the image formation process as a recursive estimation problem. We consider applying techniques in recursive estimation theory[3–5] to recursive SAR imaging. In particular, we are interested in recursive image formation of the form

$$I_k = \sum_{m=1}^{M} \alpha_m I_{k-m} + g(r_k)$$

where I_k denotes the image at time k, r_k denotes the SAR data collected at time k, $g(r_k)$ is the image contribution of the present radar measurement r_k. The computational advantage of such an approach, compared to direct computation of a block-processing CBP image formation sum, may be considerable.

Of particular interest in this paper is the image quality of a recursive image formation process, as measured by the SAR impulse response to an ideal point scattering center. We study how selection of M and of the $\{\alpha_m\}$ parameters relate to the crossrange impulse response structure. We show that for low recursion orders ($M \leq 3$), image quality metrics are similar to block-processing approaches that employ several common apodization window functions.

Corresponding author: R. Moses, E-mail: moses.2@osu.edu

Several authors have considered recursive approaches for SAR image formation.[6–8] Much of this work is focused on recursive computation of a single SAR image, rather than a tightly-coupled sequence such as a SAR video. In addition, the explicit connection between the regression parameters in the recursive sum and the crossrange impulse response behavior, as described here, appears to be new.

An outline of the paper is as follows. In Section 2 we present a recursive formulation of the convolution backprojection algorithm. Section 3 considers image quality metrics for recursive SAR; in particular, we focus on the impulse response (IPR) of the radar image and on practical sidelobe levels obtained from realistic scattering objects in the scene. Section 4 considers example responses, both for a synthetic scene and for measured imagery using the Gotcha data set.[9]

2. RECURSIVE SAR IMAGING

2.1 Backprojection Imaging

Assume a radar system interrogates a scene by transmitting a radar waveform at time τ from radar platform location $(\tilde{x}, \tilde{y}, \tilde{z}) = (\tilde{x}_\tau, \tilde{y}_\tau, \tilde{z}_\tau)$; τ is referred to as "slow time". The waveform propagates across the surveilled area and is reflected by elements in the scene. The return waveform $r_\tau(t)$ is received and recorded. This process is repeated continuously for a sequence of discrete slow times τ_j.

We are interested in forming an image on a surface. Without loss of generality, we assume the surface is centered at $(x, y, z) = (0, 0, 0)$ and furthermore that the imaging surface is predefined by the set of points (x_i, y_i, z_i). Typically, this set of points is an equally-spaced rectangular grid in the x and y dimensions, and the surface is either a horizontal surface ($z_i \equiv 0$) or a nearly-horizontal surface in which each z_i is the ground elevation of the corresponding (x_i, y_i) location—a so-called digital elevation map, or DEM.

Let $f(x, y, z)$ be the ground reflectivity function, where we assume $z = z(x, y)$ is the height of the ground at location (x, y). Then the measured return waveform $r_\tau(t)$ is given by:

$$r_\tau(t) = \int_{R^3} f(x,y,z) \int_{\omega_{\min}}^{\omega_{\max}} e^{j\omega\left(t - \frac{2}{c}\|(x,y,z)-(\tilde{x},\tilde{y},\tilde{z})\|\right)} d\omega\, dx\, dy\, dz \tag{1}$$

where c is the propagation velocity and $[\omega_{\min}, \omega_{\max}]$ is the frequency support of the range profile measurement. A standard method to recover the reflectivity from measurements is the convolution backprojection (CBP) method,[1,2] in which the estimated reflectivity $I(x, y)$ is

$$I(x,y) = \int_0^{2\pi} \int_{\omega_{\min}}^{\omega_{\max}} \tilde{r}_\phi(\omega) e^{j\omega(x\cos\phi + y\sin\phi)} |\omega| H_R(\omega)\, d\omega\, d\phi \tag{2}$$

where $H_R(\omega)$ is a range-domain apodization window (such as a Hamming or Taylor window) that has support on $[\omega_{\min}, \omega_{\max}]$ and $\tilde{r}_\phi(\omega) = \mathcal{F}\{r_\phi(t)\}$ is the Fourier transform of the range profile $r_\phi(t)$ measured over $\omega \in [\omega_{\min}, \omega_{\max}]$ at angle ϕ. Convolution backprojection is based on the idea that the one-dimensional received signal is first filtered (the convolution step), then "smeared", or backprojected along a second dimension. The convolution step is the filtering operation $\tilde{r}_\phi(\omega) \to \tilde{r}_\phi(\omega) \cdot |\omega| \cdot H_R(\omega)$. For applications in which the bandwidth is small compared to the center frequency, $|\omega| \approx 1$ and is sometimes omitted from the convolution step.

Assume that measurements are made at discrete azimuth angles ϕ_j for $j = 1, 2, \ldots$, taken at times τ_j, and that we wish to form an image $I_k(x, y)$ at time k using the J most recent radar measurements . Let us define $\hat{r}_\phi(t) = \mathcal{F}^{-1}\{r_\phi(\omega)|\omega|H_R(\omega)\}$. Then

$$I_k(x,y) = \sum_{j=0}^{J-1} \hat{r}_{\phi_{k-j}}(t(x,y)) \tag{3}$$

where $t(x, y) = 2\|(\tilde{x}_{k-j}, \tilde{y}_{k-j}, \tilde{z}_{k-j}) - (x, y, z(x, y))\|/c$ is the round-trip time delay between the radar transmitter location at time τ_{k-j} and the image location $(x, y, z(x, y))$ on the reconstruction surface. If we consider the discretized SAR image as an $N \times N$ matrix I whose ith row and lth column corresponds to position $(x_i, y_l, z(x_i, y_l))$, then we see that

$$I_k = \sum_{j=0}^{J-1} R(\hat{r}_{\phi_{k-j}}) \tag{4}$$

where the $N \times N$ matrix $R(\hat{r}_{\phi_{k-j}})$ is formed from the vector $\hat{r}_{\tau_{k-j}}$ by the smearing operation as defined in equation (3). For simplicity of notation, we drop the (x, y) indexing on the image.

In practice, the CBP imaging operation is applied on a finite window of azimuth angles which is generally (much) smaller than the 2π range suggested in equation (2). For these cases, the integral in (2) is approximated by a weighted sum, where the weighting includes an azimuth apodization window $w(\phi)$. In particular, equation (4) is modified to be

$$I_k = \sum_{j=0}^{J-1} w_{k-j} R_{k-j} \tag{5}$$

where $R_{k-j} = R(\hat{r}_{\phi_{k-j}})$ and where w_j is an angle-dependent apodization term representing samples of $w(\phi)$. For example, $\{w_j\}$ may be a Hamming or Taylor window in the azimuth direction. In addition, w_j can compensate for nonuniform angular spacing between the τ_j measurements.[10]

Direct computation of equation (5) involves $J(N^2 + C(R))$ multiplies and adds, where $C(R)$ is the number of computations needed to form R_j from the measured range profile. For the case of a general window, there does not appear to be a simple recursive formula for I_k that results in significantly fewer computations than direct computation of equation (5). If one wishes to compute I_k for every index k, direct computation using equation (5) involves significant computation and memory.

2.2 Recursive Convolution Backprojection

For the case in which measurements are continually being made, we are interested in a *recursive* formulation of the imaging process. In particular, we are interested in recursive computation of I_k in equation (5), or close approximations.

For general weighting functions $\{w_j\}$ in equation (5), direct recursive computation of I_k may impose unacceptably high requirements on computation or memory, or both. For example, to implement a rectangular weighting function

$$w_j^R = \begin{cases} 1, & 0 \le j \le J-1 \\ 0, & \text{otherwise} \end{cases} \tag{6}$$

the recursive computation of the SAR image is given by

$$I_k = I_{k-1} + R_k - R_{k-J} \tag{7}$$

The above equation requires only $2N^2$ adds per update of an $N \times N$ image; however, the memory requirement is much higher, as one needs to store J R_j matrices, or to store J $\hat{r}_{\tau_j}$ vectors and reconstruct each R_j as needed in (7). This imposes a significant cost in either computation or memory or both, especially if J is large. Moreover, for many other commonly-used windows functions, the corresponding recursive update to (5) involves significantly more computations and memory than (7), and may result in little or no computational savings over direct computation. Thus, for applications in which one wishes to compute images at finely-spaced time intervals such as for every k, exact recursions from block-processing CBP equations may be extremely expensive computationally. In order to realize a recursive computation of the SAR image, we are thus motivated to consider whether a recursive image formation method can be used, and if so, what the effective azimuth apodization window of such an approach would be.

A computationally simple recursive imaging approach is to use a first-order recursion of the form

$$I_k = \lambda I_{k-1} + R_k \tag{8}$$

where λ is an exponential forgetting factor satisfying $0 < \lambda \le 1$. The exponential forgetting recursion is often used in recursive least squares estimation[3–5] to update a covariance matrix estimate. The recursion can be shown to result in the exponentially-weighted sum and corresponding exponential window function given by

$$I_k = \sum_{j=0}^{k} \lambda^j R_{k-j} \quad \Longrightarrow w_{k-j} = \lambda^j, \quad j = 0, 1, \ldots, \tag{9}$$

Neither the exponential nor the rectangular window are commonly used for SAR image formation because of the high crossrange sidelobes that result from the step discontinuity of the window. Instead, an apodizing window which smoothly transitions from 0 to 1 to 0 for $j = 1, \ldots, J-1$ is used. Commonly-used windows include the Hamming, Taylor, or Kaiser-Bessel windows.[11]

Equation (8) can be seen as an autoregression (AR) of order 1, or AR(1) recursion. A straightforward generalization is to consider an Mth order autoregressive recursion:

$$I_k = \sum_{m=1}^{M} \alpha_m I_{k-m} + R_k \tag{10}$$

The Mth order AR recursion requires MN^2 memory locations to store the M previous images, and requires MN^2 multiplications per recursive step. In addition, the computations are well-matched for parallel or hardware implementations because, except for the computation of R_k, the multiplies and adds are carried out identically on each of the N^2 image pixel values.

The choice of M and the AR coefficients $\{\alpha_m\}_{m=1}^{M}$ determine the effective apodization window of the SAR imaging process. The azimuth window is found from the inverse Z-transform of

$$\frac{1}{A_M(z^{-1})} = \frac{1}{1 + \alpha_1 z^{-1} + \cdots + \alpha_M z^{-M}} \tag{11}$$

Specifically, $w_j = \mathcal{Z}^{-1}\left[\frac{1}{A_M(z^{-1})}\right]$.

In particular, for $M = 2$, the AR coefficients may be chosen to satisfy

$$A_2(z^{-1}) = 1 + \alpha_1 z^{-1} + \alpha_2 z^{-2} = \left(1 - \lambda e^{j\mu} z^{-1}\right)\left(1 - \lambda e^{-j\mu} z^{-1}\right) \tag{12}$$

Here, the effective azimuth window is a damped sinusoid with damping factor λ and oscillation frequency μ.

$$w_j = \beta \lambda^j \sin(j\mu), \quad j = 0, 1, \ldots \tag{13}$$

where β is a constant that does not affect the window shape. Similarly, for $M = 3$, one obtains (with two complex-conjugate poles)

$$A_3(z^{-1}) = 1 + \alpha_1 z^{-1} + \alpha_2 z^{-2} + \alpha_3 z^{-3} = \left(1 - \lambda e^{j\mu} z^{-1}\right)\left(1 - \lambda e^{-j\mu} z^{-1}\right)\left(1 - \gamma z^{-1}\right) \tag{14}$$

3. IMAGE QUALITY ANALYSIS

In this section we consider the image quality using the first, second, and third order image formation recursions, and compare with the image quality one obtains from a nonrecursive formulation with a traditional apodizing window.

For SAR imaging, one of the primary methods for assessing image quality is to define metrics from the impulse response (IPR) of the imaging operation. The IPR is the response to an ideal point scattering center at location (x_0, y_0, z_0), where usually z_0 is chosen to be on the imaging surface. Two primary measures of image quality are the mainlobe width and the sidelobe levels of the IPR.

To simplify the image quality analysis, we make two assumptions. First, we assume that the object being imaged is in the far field of the interrogating radar. Further, we assume that the image surface can be approximated as planar in the local region surrounding an object. In this case, the "smearing" operation to obtain R_k from $\hat{r}_{\phi_k}$ is locally along straight lines, and CBP imaging can be equivalently computed using the Polar Format Algorithm (PFA).[1,2] The second assumption we make is that the apodizing function applied to the image formation process is separable, or approximately separable, as a function of frequency and aspect. This is the case when the azimuth extent of measurements used to form the SAR image is modest. For many radar systems, this assumption holds true; for example, an X-band radar with center frequency of 10 GHz uses approximately 3° of

azimuth extent to form an image with 0.3m×0.3m resolution. We discuss this second assumption in more detail below.

In PFA, the imaging operation can be considered as follows: the Fourier transforms $\tilde{r}_\phi(\omega)$ of measurements $r_\phi(t)$, $R_\phi(\omega)$ are measurements along radial lines in a two-dimensional frequency space, or k-space. As the radar system moves, the measurements form a discrete measurement grid with support on a toroidal segment of k-space. The Polar Format Algorithm involves resampling these data to a rectilinear grid, applying a two-dimensional apodizing window, and computing the inverse DFT, usually using a two-dimensional FFT algorithm.

When the azimuth extent of the toroidal support region is modest, then the apodizing window is either approximately or exactly separable in the k_x and k_y directions. In this case, the mainlobe width and sidelobe levels in the downrange direction are determined by the apodizing window $H_R(\omega)$ in equation (2), while the mainlobe width and sidelobe levels in the crossrange are dictated by the azimuth apodization window, $\{w_j\}$ in equation (5). Since we are mainly interested in the effective crossrange apodization, we will focus on the crossrange response below.

3.1 Azimuth Impulse Response Characteristics

We consider first the first-order AR recursion. The azimuth window for an exponential forgetting factor is then given by

$$w(\phi_{k-j}) = \lambda^j u[j] \tag{15}$$

which, for equally-spaced $\phi_k = k\Delta\phi$ is a discrete-sample equivalent of, for continuous-valued ϕ

$$w(\phi) = e^{-\sigma\phi} u(\phi) \tag{16}$$

where $\sigma = -\ln\lambda/(\Delta\phi)$. The Fourier transform of this function is

$$\mathcal{F}[w(\phi)] = W(\Phi) = \frac{1}{j\Phi + \sigma} \tag{17}$$

whose sidelobes (for large Φ) decrease on the order of $(1/\Phi)$. This is the same behavior as a rectangular pulse $w_R(\phi)$ whose Fourier transform is a sinc function. In fact, for any rectangular window of width J samples, where J is sufficiently large, there is a corresponding value of λ given by

$$\lambda = 1 - \frac{2}{J} \tag{18}$$

whose effective crossrange mainlobe width and sidelobe response closely match those of the rectangular window. Thus, if one wishes to emulate a block-processing CPB image formation using a rectangular window with J azimuth measurements, one can use the first-order recursive recursion in (8) with $\lambda = 1 - 2/J$ as in (18).

Figure 1 shows a rectangular azimuth window and its corresponding exponential window, in both the azimuth index domain and in the corresponding Fourier transform domain. This Fourier transform domain, Φ, corresponds to the crossrange dimension in a reconstructed SAR image, and the functions shown represent the crossrange slices of the two-dimensional IPR of the SAR imaging system under the assumptions stated previously. We see that the response of the recursive window has similar mainlobe characteristics as the corresponding rectangular window response. In the sidelobe region, the crossrange response matches the "envelope" of the corresponding rectangular window sidelobe response, and has the same decay rate.

A similar analysis can be carried out for the second-order AR imaging recursion. In the bottom row of Figure 1 we compare the Bartlett (triangular) window and its corresponding crossrange response to that of a second-order AR window with μ and λ parameters in equation (12) chosen as:

$$\mu = \frac{\pi}{\frac{3}{2}J}, \quad \lambda = 1 - \frac{2}{J} \tag{19}$$

The second-order AR crossrange response has similar characteristics to the Bartlett window response because a second-order recursion has a ramp-like initial response similar to that of a Bartlett window.

To realize recursive image formation algorithms whose effective azimuth apodization window closely emulates those of commonly-used block-processing windows, a recursion of order $M = 3$ (or higher) is needed. A third-order recursion yields an impulse response whose initial behavior mimics a quadratic; such a response has a smooth first and second order derivative near zero. Figure 2 shows the effective window function, and its corresponding azimuth impulse response function, for a third-order model whose coefficients are chosen to match the behavior of a Hanning window, and one whose coefficients are chosen to match a Hamming window. The window functions and crossrange impulse responses match well for the Hanning window, somewhat less well for the Hamming window. A higher-order AR model could be chosen to realize a better match, but at the expense of corresponding higher memory and computation requirements for each update.

For the windows shown in Figure 2, the recursion parameters can be selected to match a desired window. We find that for both the Hanning and Hamming windows:

$$\mu \approx \frac{\pi}{\frac{2}{3}J}, \quad \lambda \approx 1 - \frac{2.8}{J}, \quad \gamma \approx 1 - \frac{3}{J} \tag{20}$$

(where μ, λ, and γ are defined in equation (14)) provides a close match of these block-processing windows to an effective third-order recursive window. More generally, one can solve an optimization procedure to choose the α_m parameters that "best" approximate any given block-processing window, where "best" is in the sense of minimizing some criterion such as a weighted ℓ_2 norm difference of the azimuth-domain coefficients or a weighted L_2 norm difference of their crossrange impulse response patterns.

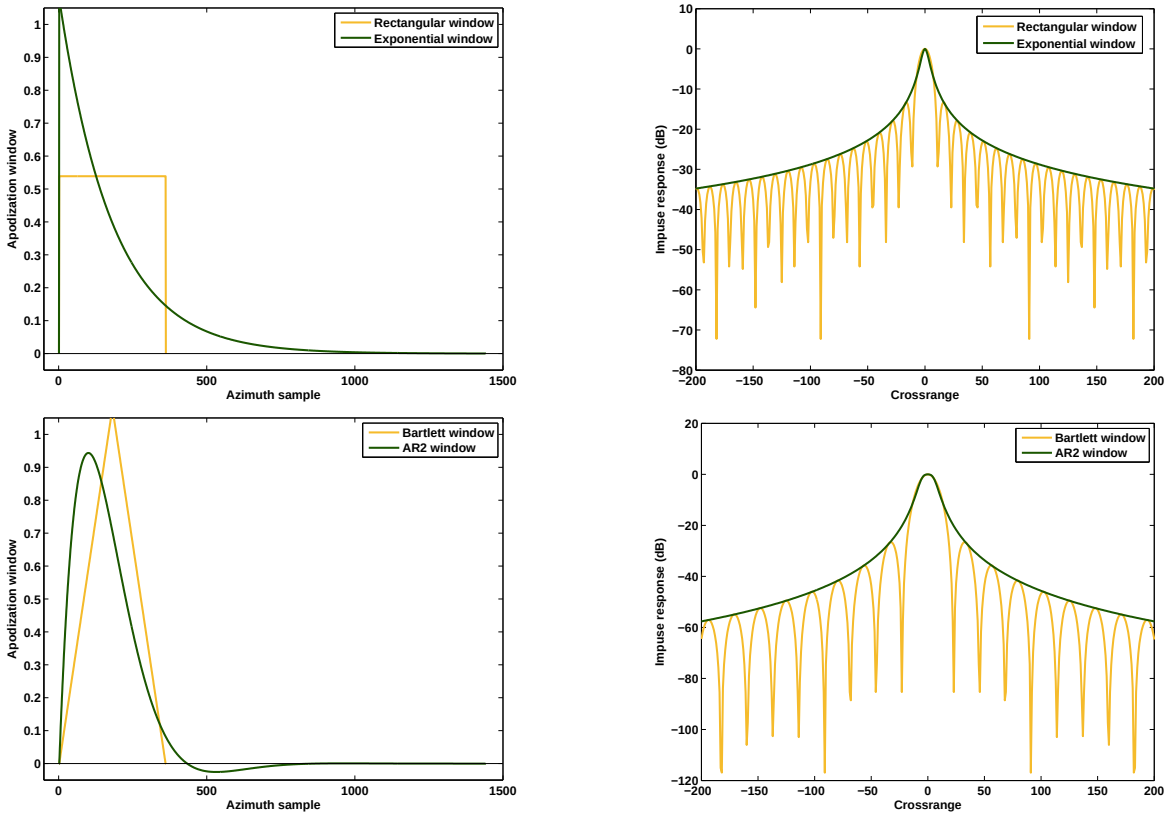

Figure 1. Azimuth windows (left) and their corresponding crossrange impulse response functions in dB (right). Top: Rectangular and AR(1) exponential window. Bottom: Bartlett and AR(2) window.

We note that with slight modification, the recursive imaging methods can accommodate significant changes in the effective azimuth window width used to form the images. As an example, Figure 3 shows three azimuth apodization windows that result from different values of $\{\alpha_1, \alpha_2\}$. The number of computations are the same, with the only change being the choice of the $\{\alpha_m\}$ parameters used in equation (10).

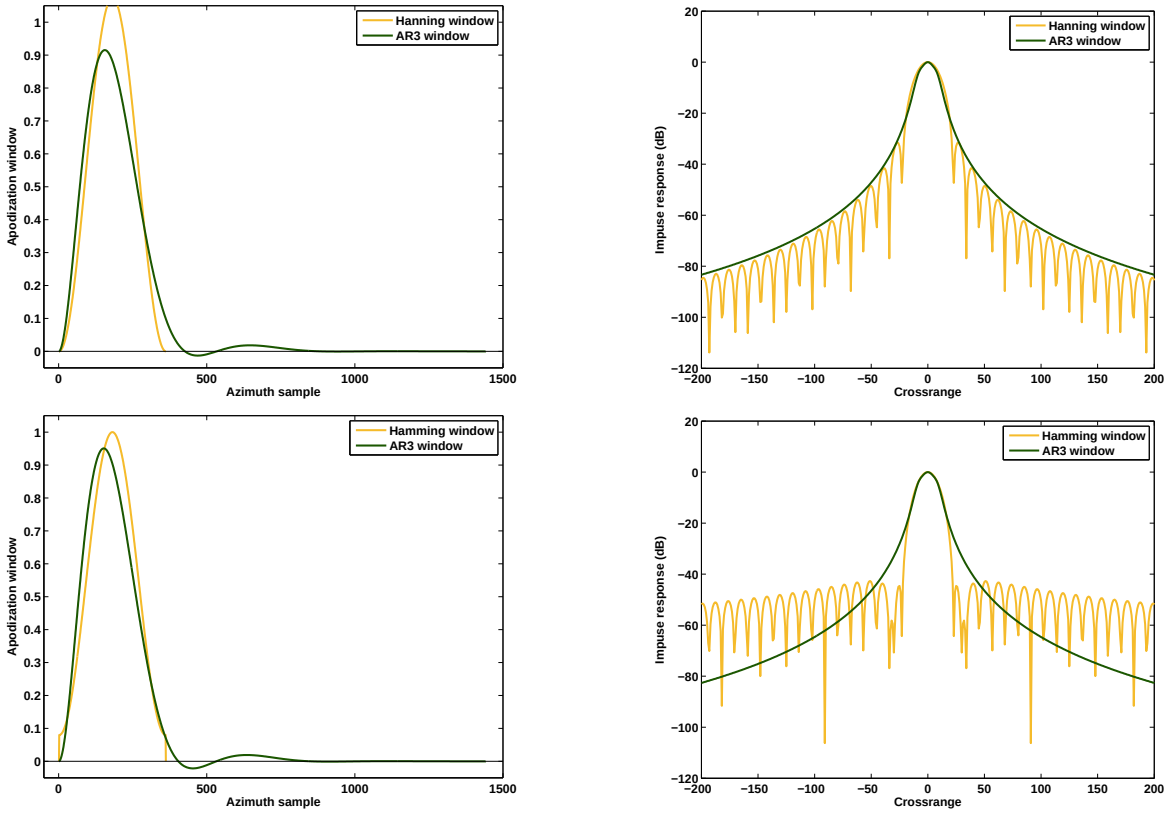

Figure 2. Azimuth windows (left) and their corresponding crossrange impulse response functions in dB (right) for third-order recursive SAR windows whose $\{\alpha_m\}$ parameters are chosen to emulate a Hanning window (top row) and Hamming window (bottom row).

3.2 Sidelobe Levels for Non-Persistent Scattering Centers

While the IPR mainlobe width and sidelobe levels are useful metrics for image quality, they may not always suggest the SAR image characteristics for practical scattering centers in the scene. The reason for this is that the IPR mainlobe width gives the crossrange resolution for a persistent scattering center over the azimuth extent of the imaging operator. In addition, the sidelobe levels seen in the IPR apply to an ideal point scatterer; that is, a scattering center whose amplitude is constant across the azimuth extent of the imaging operator, and whose phase is linear as a function of k_x and k_y. For scattering centers whose amplitude or phase do not match that of an ideal point scattering center, the true image response is the convolution of the IPR with the scattering center response function. In many cases, the sidelobe level of the convolution is (much) lower than that of the IPR function itself.

To illustrate this point, consider a scattering center whose response amplitude varies with azimuth as a Gaussian amplitude profile, as shown in Figure 4. Such a response might arise from an object with nonzero length, such as a dihedral or side of a building.[12] In this figure, we consider a scattering center with linear phase but a Gaussian amplitude profile, and being imaged recursively with an imaging operator using an exponential azimuth weighting function as in equation (9). Shown in the bottom row are crossrange response slices of the two-dimensional SAR impulse response functions, taken along the downrange distance of the scattering center, for four different SAR images corresponding to four azimuth apertures. The four azimuth apertures are shown by the light-colored exponential windows in the top row. These four apertures can be considered as four time snapshots of a time-updated SAR video. For comparison, the crossrange response function corresponding to the exponential window is shown in the bottom row of plots as the light-colored line.

When the discontinuity of the exponential window in Figure 4 overlaps the large-amplitude region of the scattering response, as shown in the second column of plots in the figure, the azimuth sidelobes are high.

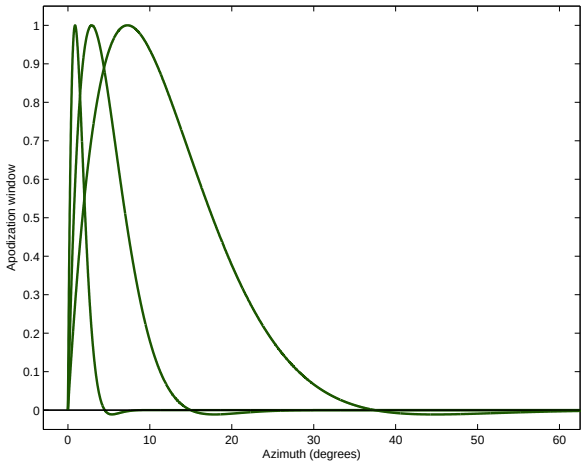

Figure 3. Three aperture windows corresponding to three sets of $\{\alpha_1, \alpha_2\}$ parameter pairs in the second-order recursive image formation. The selection $\{\alpha_1, \alpha_2\} = (1.983, -0.983)$ gives a 3-degree window, $\{\alpha_1, \alpha_2\} = (1.995, -0.995)$ gives a 15-degree window, and $\{\alpha_1, \alpha_2\} = (1.998, -0.998)$ gives a 35-degree window.

However, when the exponential window is to the left of the scattering center (as in the first column), or when the window includes most or all of the scattering center response, as in the right two columns, the sidelobes are much lower, about 35 dB below the peak response in the example shown. In this latter region, the sidelobe response is primarily dictated by the scattering object's azimuth response, not by the apodization window. If the SAR image were displayed as a video, one would expect high sidelobe 'flashes' to be limited to these short transient events. For video SAR applications, such transient high-sidelobe events may be acceptable if they occur for a relatively short transient time.

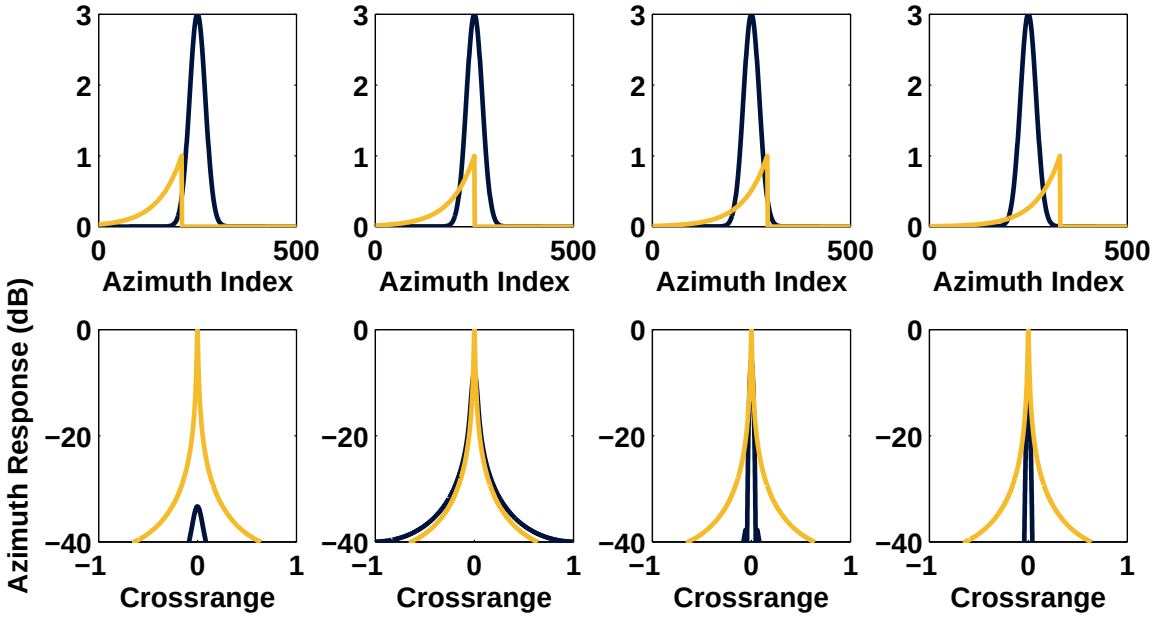

Figure 4. For scattering centers with limited persistence, high sidelobes are seen only during the transient period in which the window overlaps only part of the response (2nd from left). Shown are the azimuth amplitude of the scattering center (top row, blue) and the exponential window corresponding to a recursive SAR image at four 'current' values of azimuth (top, yellow). The bottom row shows the azimuth response of the scattering center (blue) at the range of the scattering center, in dB. For comparison, the azimuth response of the exponential window is also shown (yellow).

For scattering centers with large azimuth persistence angles, such as tophats, trihedrals, and spheres, the azimuth sidelobes are dominated by the azimuth IPR response of the SAR imaging operator; for these types of scattering centers, one would expect a crossrange response similar to the responses given in Figures 1 and 2.

4. NUMERICAL RESULTS

In this section we present numerical results comparing traditional, nonrecursive SAR images with those obtained using the recursive update equations. We consider first a synthetic SAR scene consisting of several canonical scattering shapes, and then present results using the Gotcha public release dataset.[9]

4.1 Synthetic Scene

We first present results using synthetic SAR data of a scene containing several canonical scattering shapes. The 20m $\times$ 20m scene is shown in Figure 5. Six canonical scattering objects are in the scene, namely (from top to bottom and left to right) a 2 meter dihedral, a tophat with 1 meter radius, two ideal point scatterers, a trihedral with 2 meter edges, and an ellipsoid (elongated sphere) with major and minor radii of 2.5 meters and 1 meter, respectively. The peak amplitudes of these scattering responses were (artifically) set to be equal so that all could be clearly seen in the images.

We simulate a radar whose center frequency is 9.6 GHz and bandwidth is 640 MHz. The radar traverses a circular path of radius 10km from scene center. Measurements are taken in equal azimuth increments, with azimuth spacing of $\frac{1}{120}^\circ$. These are approximately the radar measurement parameters of the Gotcha data presented in Section 4.2.

We form SAR images of the synthetic data in four ways. We form standard, block-processing SAR images using a convolution backprojection algorithm with both a rectangular azimuth window and a Hamming azimuth window. In both cases we use a 3° aperture, so $J = 360$. We also form two recursive images, using both the first-order recursion with λ chosen using equation (18) and the third-order recursion with μ, λ, and γ chosen using equation (20). These images can be considered as snapshots of SAR videos.

Figure 5 shows four SAR images for an azimuth centered at 45°; here, the radar is located in the direction of the top-right corner of the images. We see good agreement between the responses of the rectangular window and the first-order recursive estimate; the rectangular window sidelobes are oscillatory, while the envelopes of the recursively-formed images are smooth, but the crossrange sidelobes decay at the same rate. The downrange responses are similar, because the same (Hamming) downrange apodization window $H_R(\omega)$ was applied to the measurements in all four cases. The third-order AR and Hamming-weighted images are also similar to each other. The Hamming-weighted image shows slightly wider crossrange responses, and slightly lower sidelobes, than the third-order AR image, which is consistent with the crossrange IPR slices shown in Figure 2.

4.2 Gotcha Data Set

In this section we present results of block-processing and recursive imaging using measured SAR data from the Gotcha Public Release dataset.[9] The Gotcha radar data has a center frequency of 9.6 GHz, a bandwidth of 640 MHz, and an azimuth measurement sampling in azimuth of approximately $1/120^\circ$. For this data, the radar flies a circular path with a radius of approximately 10 km from scene center, at a nominal elevation angle of 45°.

Figure 6 shows two snapshot images from SAR videos of a parking lot containing several vehicles from the Gotcha data set. Block-processing Hamming-weighted CBP images were formed using an azimuth extent of 3°, and recursive images using the AR(3) parameters as in equation (20) were generated. As can be seen, these images are quite similar to each other.

As mentioned previously, the recursive imaging methods can accommodate significant changes in the effective azimuth window width used to form the images simply by changing the $\{a_m\}$ parameters used in the recursion. To illustrate this, Figure 7 shows a snapshot of the third-order recursive Gotcha image sequence, where the recursion coefficients were in this case chosen to give an effective azimuth window whose width is approximately 25°. The computations are the same as those used to form Figure 6(b), with the only change being the choice of the $\{\alpha_m\}$ parameters used in equation (10).

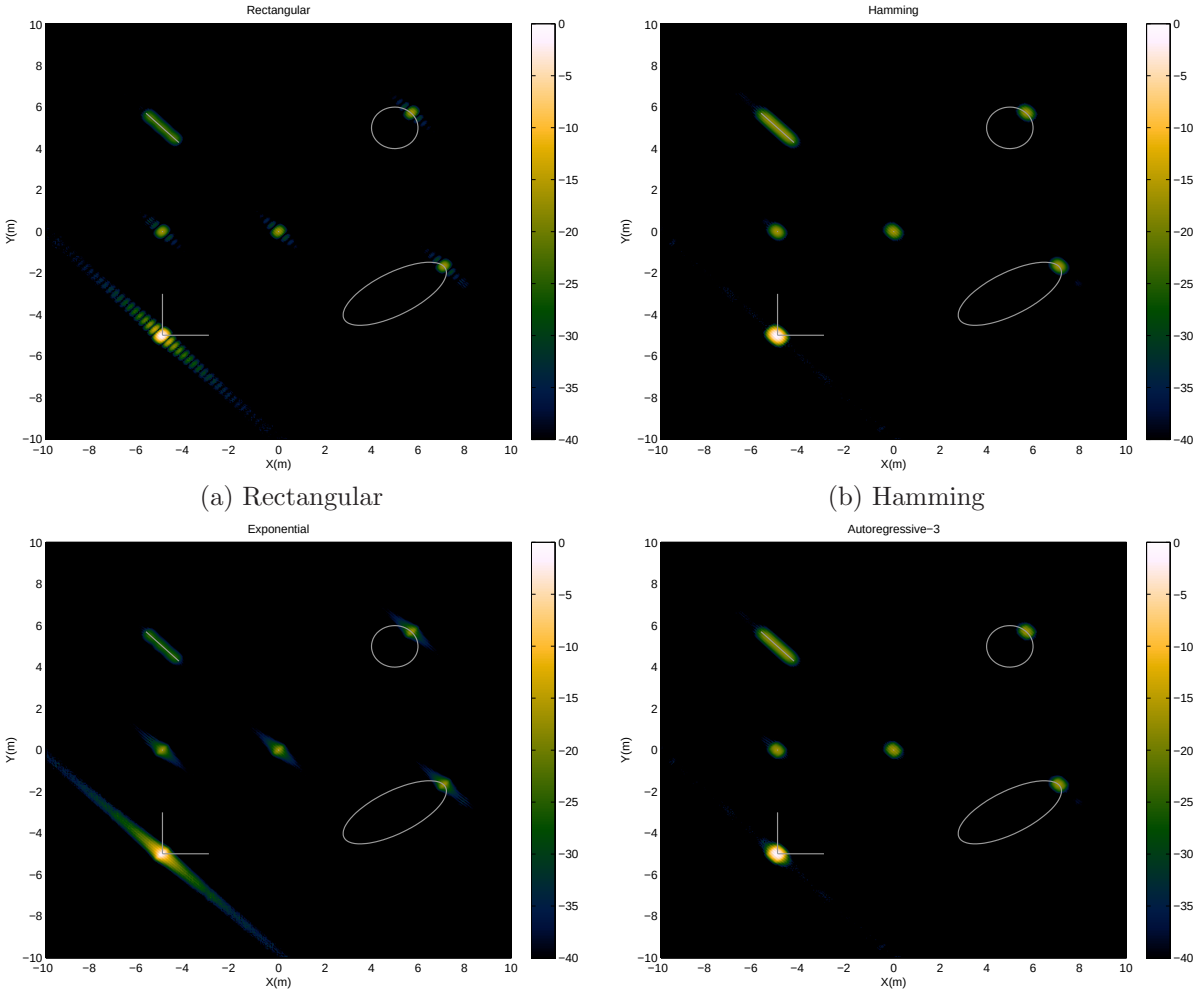

(a) Rectangular (b) Hamming

(c) AR(1) (d) AR(3)

Figure 5. SAR images of a synthetic scene consisting of six canonical scattering shapes. The top two images are formed using block-processing methods with a rectangular and Hamming azimuth window. The bottom two images are formed recursively using a first-order and third-order recursion. The azimuth windows of all four methods are those in Figure 1 and 2. The image resolution is approximately 0.3m×0.3m.

5. CONCLUSIONS

We have presented an approach for recursively computing backprojection SAR imagery, using a low-order autoregression. After each radar measurement is obtained, the SAR image is updated as a linear combination of M past values of the image and the current convolved and backprojected measurement. The number of multiplies is on the order of MN^2, where N^2 is the number of image pixels. In addition, the storage requirement is approximately $(M+1)N^2$ complex numbers. This recursive update involves significantly fewer computations than is needed for block processing computations of successive SAR images, and is therefore well-suited for applications in which composite videos of successive SAR images is desired.

We have studied the effective azimuth apodization window that can be obtained for low-order ($M \leq 3$) recursive updates. A first-order update fits closely to a rectangular window. A second-order recursion, with appropriate choice of recursion parameters, can be made to approximate a Bartlett (triangular) window, and with a third-order recursion one can select regression coefficients to closely approximate a Hanning window, and can select coefficients to somewhat less closely approximate a Hamming window.

An important property of the recursive window is that simply by changing the scalar autoregressive coeffi-

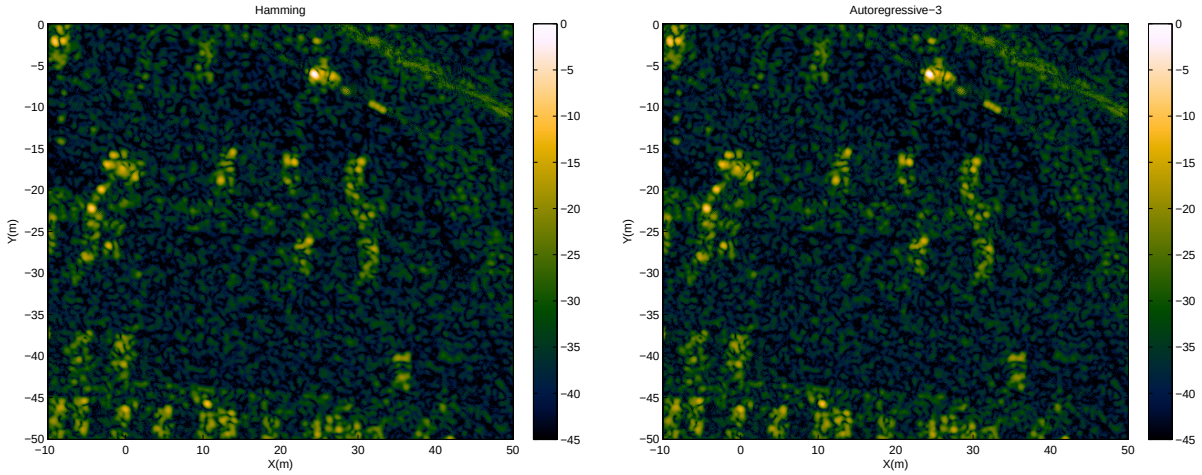

(a) Hamming (b) AR(3)

Figure 6. SAR images of a parking lot using phase history data from the Gotcha Public Data Set. (a) Block-processing image using the Hamming azimuth window. (b) Third-order recursive image. The azimuth windows are those in Figure 2. The image resolution is approximately 0.3m×0.3m.

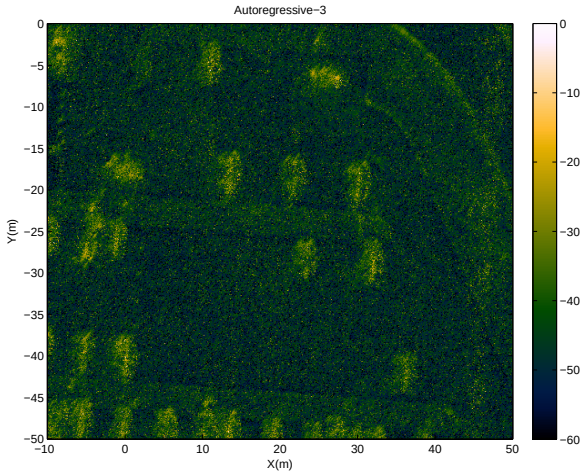

Figure 7. SAR image of a parking lot using phase history data from the Gotcha Public Data Set. The image is formed using a third-order recursion, with coefficients selected to give an azimuth window whose width is approximately 25°.

cients in the recursion, the effective azimuth integration width of the SAR image can be adjusted. Thus, SAR images that integrate over, say, 3 degrees or 25 degrees of aperture involve the same number and same type of computations; only the M $\{\alpha_m\}$ scalars in the recursive update equation are changed. This allows for on-the-fly changing of aperture, or for forming images at multiple aperture widths, with modest additional computation and memory requirements.

6. ACKNOWLEDGEMENTS

This material is based upon work supported by a MURI award from the the Air Force Office of Scientific Research under Award No. FA9550-06-1-0324. Any opinions, findings, and conclusions or recommendations expressed in this publication are those of the authors and do not necessarily reflect the views of the Air Force.

REFERENCES

1. C.V. Jakowatz, D.E. Wahl and P.H. Eichel, *Spotlight-Mode Synthetic Aperture Radar: A Signal Processing Approach*, Kluwer Academic Publishers, Boston, MA, 1996.
2. W. G. Carrara, R. S. Goodman, and R. J. Majewski, *Spotlight Synthetic Aperture Radar: Signal Processing Algorithms*, Artech House, Norwood, MA, 1995.
3. T. Söderström and P. Stoica, *System Identification*, Prentice-Hall, London, 1989.
4. S. Haykin, *Adaptive Filter Thoery (4th edition)*, Prentice-Hall, New Jersey, 2002.
5. T. Kailath, A. H. Sayed, and B. Hassibi, *Linear Estimation*, Prentice Hall, New Jersey, 2000.
6. A. Farina and C. F. Morabito, "Recursive system for image forming by means of a spotlight synthetic aperture radar," European Patent No. EP0409219A2, Jan. 23, 1991.
7. H. Hellsten, "A synthetic aperture radar," International Patent No. WO 92/16856, Oct. 1, 1992.
8. T. Shirakawa, H. Kitajima, Y. Ogawa, and T. Shimono, "SAR image reconstruction using a Kalman filter," *Electronics and Communications in Japan, Part 3* **77**(10), pp. 85–92, 1994.
9. "Gotcha Volumetric SAR data set, Version 1.0," 2007. https://www.sdms.afrl.af.mil/datasets/gotcha.index.php.
10. J. Tangudu, "Back projection algorithms for ultra wide band radar imaging," Master's thesis, The Ohio State University, August 2000.
11. P. Stoica and R. L. Moses, *Spectral Analysis of Signals*, Prentice-Hall, New Jersey, 2005.
12. L. C. Trintinalia, R. Bhalla, and H. Ling, "Scattering center parameterization of wide-angle backscattered data using adaptive Gaussian representation," **45**, pp. 1664–1668, Nov. 1997.